Time dependent thermal lensing measurements of V–T energy transfer from highly excited NO_2

Beatriz M. Toselli,[a] Theresa L. Walunas,[b] and John R. Barker[c]
Department of Atmospheric, Oceanic, and Space Sciences, Space Physics Research Laboratory, The University of Michigan, Ann Arbor, Michigan 48109-2143

(Received 27 November 1989; accepted 10 January 1990)

The time dependent thermal lensing technique has been used to measure the vibrational relaxation of NO_2 (initially excited at 21 631 cm^{-1}) by Ar, Kr, and Xe. The energy transfer analysis was carried out in terms of $\langle\langle \Delta E \rangle\rangle$, the bulk average energy transferred per collision. This quantity was found to have a very strong dependence on vibrational energy, with a marked increase at energies greater than about 10 000 cm^{-1}, where several electronic excited states ($^2B_2$, $^2B_1$, and $^2A_2$) mix with the ground state ($^2A_1$). This effect may be due to large amplitude vibrational motions associated with the coupled electronic states. Even at low energies, deactivation is faster than in other triatomic systems, probably because NO_2 is an open shell molecule and electronic curve crossings provide efficient pathways for vibrational deactivation. The V–T rate constant for deactivation of $NO_2(010)$ by argon is estimated to be $(5.1 \pm 1.0) \times 10^{-14}$ cm^3 s^{-1}. Results obtained for NO_2^*–NO_2 collisions gave $\langle\langle \Delta E \rangle\rangle$ values in good agreement with literature results from fluorescence quenching experiments, indicating that V–T may be more important than V–V energy transfer in the quenching process.

I. INTRODUCTION

Energy transfer in highly excited molecules can be studied using several physical techniques, instead of the traditional unimolecular reaction systems. The physical techniques are advantageous, because they avoid complications due to chemical reaction mechanisms and they can be applied at energies lower than reaction thresholds. Most physical techniques depend crucially on accurate calibrations, which are confined to the specific system studied. In our laboratory, time-resolved infrared fluorescence has been used to measure energy transfer involving azulene,[1,2] 112-trifluoro ethane,[3] and benzene[4] molecules, after laser excitation. Troe and coworkers have used time-resolved ultraviolet absorption to study energy transfer in large polyatomic molecules,[5,6] CF_3I,[7] and the triatomics SO_2[8] and CS_2.[9] A weakness of these methods is that the calibration is very important and must be carried out for each separate system studied. Spectroscopic techniques also require detailed spectroscopic data for each system studied. For example, infrared fluorescence from NO_2 excited at 400–500 nm recently was used to determine the quenching rate constants for deactivation by NO_2 and several other gases.[10]

An alternative to physical techniques that require individual calibrations are photothermal techniques, which depend almost exclusively on laser beam characteristics and on the properties of the collider gas, rather than those of the excited molecule. Such techniques include time-dependent thermal lensing (TDTL),[11–14] time-resolved optoacoustics,[13,15] UV absorption by a tracer gas,[16] and the probe beam deflection technique.[17]

In this paper we present TDTL measurements of V–T energy transfer in NO_2 initially excited at 21 631 cm^{-1}, in the presence of Ar, Kr, and Xe. NO_2 has been the object of innumerable studies, partly because it is one of the few chemically stable gaseous species of unpaired electronic spin, and partly because of its strong and complex absorption in the visible.[18] The notorious complexity of the visible spectrum of NO_2 has been attributed to strong perturbations of the electronic excited states ($^2B_2$, $^2B_1$) by vibronic coupling with high-lying levels of the electronic ground state ($^2A_1$). NO_2, SO_2, and CS_2 are members of a class of molecules with overlapping electronic states, which exhibit much longer radiative lifetimes than would be expected from their measured integrated absorption coefficients, as was first discussed by Douglas.[19]

Despite the large number of studies involving the NO_2 molecule (which cannot be reviewed here) the understanding of energy transfer in this system is far from complete. Although the visible fluorescence of NO_2 has been studied extensively by Kaufman and coworkers,[20] and information has been obtained about the vibrational quenching rates for NO_2 at high levels of excitation, there is only one paper reporting direct measurements of energy transfer that may apply to lower energies, and the interpretation of those results is not straightforward.[10]

The main goal of the present work is to elucidate collisional deactivation processes in NO_2 at intermediate and low energies. The TDTL technique was employed because it monitors the energy transfer to the translational degrees of freedom and is independent of the extremely complex spectroscopy of NO_2. Furthermore, the technique can be extended to other excited molecules, without the necessity of carrying out additional calibrations. Despite some limitations of the technique, which are described in detail, considerable information was obtained about the NO_2 system.

II. EXPERIMENT

NO_2 (Matheson) was stored in a blackened container after it was purified by mixing with O_2 overnight, followed

[a] Postdoctoral research associate
[b] Participant in the NSF Research Experience for Undergraduates program.
[c] Also Department of Chemistry

 0021-9606/90/084793-12$03.00

by freezing at dry ice temperature and pumping to eliminate O_2 and other volatile impurities, until the solid was completely white. The rare gas diluents were cylinder gases of research grade and were used without further purification. All the experiments were carried out at room temperature.

The NO_2 molecules absorb some of the energy from the pulsed laser beam and then the absorbed energy is transferred by collision to the translational and rotational degrees of freedom as heat. This energy deposition results in a temperature rise and concomitant reduction in gas density at the center of the beam, but less change away from the center. The change in the gas density produces a variation in the refractive index (a lens), which dissipates at longer times due to thermal conductivity. The sign and magnitude of the time dependent lensing effect are measured by using a pinhole and photomultiplier to monitor the light intensity at the center of a CW He–Ne laser beam, that is counter-propagated with the pump laser. A schematic of the optical setup is shown in Fig. 1. The counter-propagating geometry was chosen to reduce the effects of scattered light from the pump laser, which is many times more intense than the probe laser. Although this geometry is very helpful in reducing interference from the pump laser, accurate coaxial alignment of the two laser beams is nontrivial.

Descriptions of many experimental details can be found in Ref. 12 and 13. Visible light (462.3 nm) from the pulsed tunable dye laser (Lumonics Hyperdye-300, using Coumarin 460 dye) pumped by a XeCl excimer laser (Lumonics Hyperex 400) was directed through a cell containing a mixture of NO_2 and a buffer gas (usual ratio of 1:5000). The energy of the dye laser (typically 3 mJ pulse^{-1}; see Table II) was continuously monitored with a Scientech absorbing calorimeter power meter at the position shown in Fig. 1. For a typical pulse length of $\sim$20 ns, this energy corresponds to $\sim$150 kW, compared with the $\sim$0.5 mW He/Ne probe laser (Spectra-Physics, Model 155A). Scattered light from the probe laser was virtually eliminated by filtering with a 6328 Å interference filter and using a 0.5 m Ebert monochromator equipped with a R955HA photomultiplier.

The laser beams were combined and separated on quartz-flat beam splitters. To aid in optical alignment, two irises were placed as shown in Fig. 1. After alignment was complete in each experimental run, the irises were opened wide in order to avoid spurious effects due to Fresnel diffraction.

For the pump laser, a well-defined Gaussian beam is desirable, because the initial spatial distribution of the excited molecules depends on the pump laser beam spatial profile and the theory of the TDTL experiment is most easily applied for Gaussian profiles. Even if the pump laser beam is not Gaussian, the theory can be applied to arbitrary profiles, as long as they are axially symmetric. Unfortunately, the pump laser (Lumonics Hyperdye-300) used in the experiments is pumped through a side window and the beam profile is neither Gaussian, nor axially symmetric, but it has a somewhat triangular to rectangular cross section. The intensity profile of the beam was determined by scanning the beam with a pinhole and photodiode. The beam profile showed an approximately Gaussian shape, but with some superimposed structure and some satellite peaks near the wings. These irregularities can affect the initial TDTL signal shape, but will be gradually eliminated due to thermal conductivity and diffusion of excited molecules in the course of time. As shown below, the theory (based on Gaussian profiles) and experiments showed small differences during the first 5–10 μs, but the discrepancies were minor and did not affect the energy transfer results.

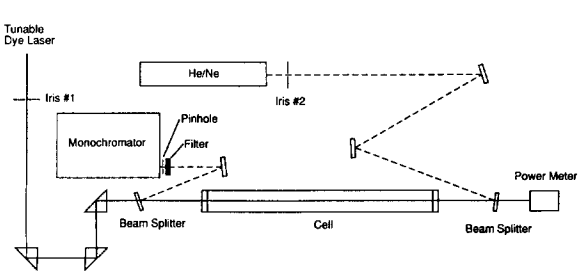

FIG. 1. Experimental apparatus used in the TDTL technique.

The time dependent signals were amplified with a Tektronix AM 502 dc-coupled amplifier and averaged with a LeCroy 9400 digital oscilloscope for 10 000–50 000 laser pulses in each experiment. The signal was further analyzed after transfer to a Macintosh personal computer. TDTL signals were obtained as a function of the inert gas pressure from 10 to 500 Torr and simulated using a theory that incorporates all the gas-dynamics factors that affect the density in the system. A brief outline of the theory is presented in the next section.

III. TDTL THEORY

The theory of TDTL has been discussed by Flynn and coworkers,[11] by Bailey and coworkers,[21] by Barker and coworkers,[12,13] and recently by Jacobs,[22] who has presented an accurate numerical method for solving the governing equations for this photothermal system. The following presentation of the TDTL theory is based on the review article from Ref. 13, and the reader should consult that reference and the articles cited there for more details.

After the absorption of the laser radiation the gas-dynamic factors that affect the TDTL signal are: 1) the energy-deposition rate to produce translational heat, 2) the acoustic waves generated by the heat deposition, 3) the binary diffusion of the excited molecules through the bath gas, 4) the thermal conductivity, and 5) the viscosity. In the following analysis, viscosity has been neglected, because its effect is unimportant, as shown by Jacobs.[22] The magnitude of the thermal lensing effect depends on the competition between the rate of creation of the lens due to V–T energy transfer and the rate of decay of the lens due to the gas-dynamic factors. It is useful to consider the time scales associated with each of these processes.

The time scale for V–T energy transfer can be defined considering a two level system

$$A^* + M \rightarrow A + M, \tag{1}$$

where A^* is the excited molecule and M is the collider gas. The heat deposition process is characterized by the time con-

stant

$$\tau_e = (k_1[M])^{-1} = k_e^{-1}, \tag{2}$$

where k_1 is the bimolecular rate constant, k_e is the corresponding pseudo-first order rate constant, and $[M]$ is the collider gas concentration.

For acoustic waves the acoustic transit time across the laser beam is

$$\tau_s = \frac{r_b}{c}, \tag{3}$$

where c is the speed of sound and r_b is a parameter that characterizes the radius of the pump-laser beam and is very important in controlling the shape of the TDTL signal, as discussed below.

The characteristic time scale for diffusion of excited species is

$$\tau_d = \frac{r_b^2}{4D_{12}}, \tag{4}$$

where D_{12} is the binary diffusion coefficient.

According to Bailey *et al.*[21] the time scale for thermal conductivity is

$$\tau_t = \frac{PC_p r_b^2}{4RT\lambda}, \tag{5}$$

where P is the total pressure, C_p is the molar heat capacity at constant pressure, R is the gas law constant, T is temperature, and λ is the thermal conductivity coefficient.

In energy transfer studies, it is desirable that the energy transfer time scale be well separated from the others, leading to the following idealized guidelines:

$$\tau_t, \tau_d > 10\tau_e > 100\tau_s. \tag{6}$$

For most polyatomic systems of interest, however, the conditions given by Eq. (6) are rarely met and the only way to extract the rate constant for energy transfer from the TDTL experiments is by comparisons with simulations that take into account all the gas-dynamic processes. This is the approach followed in the present work.

The transient lensing signal S is defined as

$$S = 1 - I/I_o, \tag{7}$$

where I_o is the intensity at the center of the unperturbed He–Ne laser probe laser beam at the position of the pinhole, and I is the corresponding time dependent intensity when the lens is present. For small signals ($< 15\%$) and when the pinhole radius is much smaller than the laser beam radius, it has been shown[21] that

$$S = \left(\frac{Z^2}{n_0}\right)\left(\frac{\partial^2 n}{\partial r^2}\right)_{r=0}, \tag{8}$$

where n_o and n are the refractive indices of the unperturbed and perturbed gas, respectively, and r is the radial distance from the optical axis. For a large signal and for the case when the pinhole is located some distance from the exit of the cell, Eq. (8) becomes[13]

$$S = 1 - [\cosh(\xi^{1/2}Z) + \xi^{1/2}L\sinh(\xi^{1/2}Z)]^{-2} \quad \xi > 0, \tag{9a}$$

$$S = 1 - [\cos(|\xi|^{1/2}Z) - |\xi|^{1/2}L\sin(|\xi|^{1/2}Z)]^{-2} \quad \xi < 0. \tag{9b}$$

[Note that Eqs. (9a) and (9b) differ by a factor $\xi^{1/2}$ from that in Ref. 13, where this factor was inadvertently omitted.] In these equations, Z represents the cell length and L is the distance from the exit of the cell to the pinhole. When L can be neglected, these expressions reduce to

$$S = [\tanh(\xi^{1/2}Z)]^2 \quad \xi > 0 \tag{10a}$$

$$S = [\tan(|\xi|^{1/2}Z)]^2 \quad \xi < 0, \tag{10b}$$

where

$$\xi = \frac{1}{n_0}\left(\frac{\partial^2 n}{\partial r^2}\right)_{r=0}. \tag{11}$$

The simulations we present in this paper were carried out using Eq. 10. For our experimental conditions, the shape of the signal, and therefore the energy transfer parameters we extracted, were not affected by the sinh term in Eq. 9 as confirmed by direct calculation. However, note that for large signals (> 0.5) and/or for very large L, the sinh term will affect not only the magnitude of the signal but its shape.

The refractive index is related to the gas density (ρ) by the Lorentz–Lorenz law,[23] leading to the final expression for the TDTL signal:

$$S = \tanh\left\{\left[\frac{3A}{2M}\left(\frac{\partial^2 \rho}{\partial r^2}\right)_{r=0}\right]^{1/2} Z\right\}^2, \tag{12}$$

where A is the molar refractivity and M is the molecular weight of the gas. The density fluctuation due to energy transfer can be obtained by solving numerically the gas dynamic equations for mass, energy, and momentum. These equations are combined, linearized, and manipulated to produce a third-order partial differential equation for the density as a function of position and time.[12,13] By expanding the density in terms of zero-order Bessel functions (for convenience in obtaining a tractable solution), the partial differential equation is transformed to an ordinary differential equation which can be solved by Laplace transforms, using the initial conditions.[12,13] As pointed out by Jacobs,[22] use of the zero-order Bessel functions imposes incorrect boundary conditions, leading to a phase-error in the calculated reflected acoustic waves. Except for this deficiency, the Laplace transform solution gives very accurate results and is very computationally efficient.

The original theory derived in Refs. 12 and 13 assumes that the rate constant for V–T energy transfer is a constant. For a two-state system, this will be true, but for a molecule with many vibrational states, the effective rate constant is expected to be a function of vibrational energy, which changes as a function of time. For molecules with high vibrational state densities, elementary V–T rate constants are rarely accessible and it becomes more practical to describe energy transfer in terms of the average amount of energy transferred per collision. When averaged over the population distribution, which is evolving with time, it is necessary to discuss the time-dependent bulk average energy transferred per collision: $\langle\langle \Delta E(t) \rangle\rangle$. This quantity, in a multiple state system undergoing an energy cascade, can be related to an effective V–T rate constant in an effective two-state system (appropriate for the theory), as follows.

The TDTL signal is sensitive only to the energy deposited in the translational degrees of freedom. For a monatomic

collider gas, the rate of translational energy deposition can be related to the average rate of loss of vibrational energy:

$$\frac{dq}{dt} = -\frac{d}{dt}\langle\langle E\rangle\rangle. \tag{13}$$

In the two-state system, the rate of energy loss from the ensemble of excited molecules is

$$\frac{d}{dt}\langle\langle E\rangle\rangle = H_1\frac{d}{dt}N_1 = -H_1k_eN_1, \tag{14}$$

where $\langle\langle E\rangle\rangle$ is the bulk average energy, N_1 is the number density of excited molecules, H_1 is the difference in enthalpy between the upper and lower states, and k_e is the pseudo-first order rate constant for energy transfer in Eq. (2). Since the excitation energy in the ensemble of excited molecules is just $\langle\langle E\rangle\rangle = H_1N_1$, Eq. (14) can be written

$$\frac{d}{dt}\langle\langle E\rangle\rangle = -k_e\langle\langle E\rangle\rangle. \tag{15}$$

By definition, the rate of change of $\langle\langle E\rangle\rangle$ is given in terms of $\langle\langle \Delta E\rangle\rangle$ by

$$\frac{d}{dt}\langle\langle E\rangle\rangle = k_{LJ}N_c\langle\langle \Delta E(t)\rangle\rangle, \tag{16}$$

where k_{LJ} is the bimolecular rate constant for collisions (assuming Lennard–Jones potentials) and N_c is the collider gas number density. Thus, the rate constant for energy transfer is expected to be time-dependent:

$$k_e(t) = -k_{LJ}N_c\frac{\langle\langle \Delta E(t)\rangle\rangle}{\langle\langle E(t)\rangle\rangle}. \tag{17}$$

In the simulations, a functional form must be assumed for $\langle\langle \Delta E(t)\rangle\rangle$, or for $k_e(t)$. Furthermore, the excitation energy $\langle\langle E(t)\rangle\rangle$ residing in the excited molecules at any time can be calculated by numerically integrating Eq. (15). Thus, $\langle\langle \Delta E\rangle\rangle$ can be expressed as a function of the corresponding energy $\langle\langle E\rangle\rangle$. For modeling the data, it was convenient to assume $k_e(t)$ is given by the empirical expression:

$$k_e = k_o\exp(-A\omega t) + k_1\exp(-B\omega t) + k_{\text{lim}}, \tag{18}$$

where $\omega = k_{LJ}N_c$ is the collision frequency. The parameters k_o, A, k_1, B, and k_{lim} are adjusted empirically to obtain agreement between the simulations and experiments. Equation (18) was found to be the simplest expression adequate to simulate the experimental data. Note that Eq. (18) permits analytical integration of Eq. (15).

The TDTL theory described above can applied for any arbitrary time interval, if it is assumed that k_e is constant during the interval and if the initial conditions for the interval are accounted for properly. The only difference from the original theory is that now for each time step the derivative of the coefficients for the Bessel function expansion of the density fluctuation must be evaluated in order to advance the solution. At time zero, the derivatives are equal to zero, but at later times, the spatial distribution evolves and the derivatives vary with time. The results of this approach were compared with the exact solution using the program DIFCOLL kindly provided to us by S. Jacobs,[22] and both treatments produce exactly the same results (except for the reflected acoustic waves), when sufficiently small time steps are taken.

For comparison with the experimental data, the instrument response function, which depends on the electronics and photomultiplier load resistor, was numerically convolved with the theoretical calculations. For the detailed comparisons with experimental data near the initial acoustic wave spike, this step was necessary, because the electronics introduced small delay times and the photomultiplier time response (with 1200 Ω termination) was about 0.1 μs.

IV. TDTL SIGNALS

It is interesting to analyze TDTL signals to determine how they are affected by energy transfer, acoustic waves, diffusion, and thermal conductivity. In Fig. 2 are shown TDTL signals for a mixture of 0.04 Torr of NO_2 and 200 Torr of Ar, Kr, and Xe (See Table I for the physical properties of the gases). Note that despite the similarities of the signals, each shows the effects of atomic mass on the thermal conductivity and diffusion coefficients (Table I). The magnitude of the signal under the same conditions depends on the optical properties of each inert gas, especially the molar refractivity, which explains why the signal for Xe is largest.

The optical and physical properties of the collider gases are very important in determining the feasibility of the TDTL technique for energy transfer measurements, in addition to the properties of the excited molecule under study. For example, He and Ne thermal conductivities are so large that thermal conduction is the most important factor controlling the signal at all times, and energy transfer could not be measured. Moreover, the low molar refractivities of these gases produced small signal amplitudes and usable signals could not be obtained at the high dilution ratios necessary.

The initial rising portion of the signals is controlled mostly by the rate of energy transfer and by acoustic waves, while the decaying portion is dominated by thermal conductivity. Diffusion plays a small role throughout. The initial spike observed in all of the signals occurs because part of the

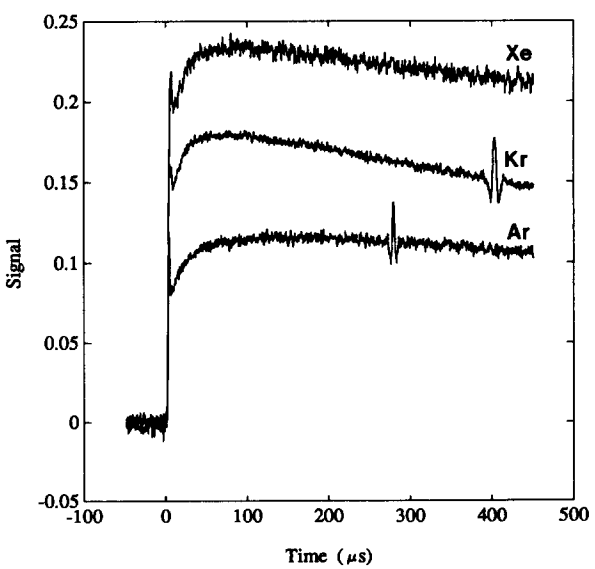

FIG. 2. Typical experimental TDTL signals for a mixture of NO_2 (0.04 Torr) and Xe, Kr, or Ar ($\approx$200 Torr) in order of decreasing intensity. See Table II for the physical conditions.

TABLE I. Physical properties. $T = 298$ K.

	σ_{LJ} (Å)	ε/k (K)	k_{LJ} ($cm^3 s^{-1}$)	λ (cal $K^{-1} s^{-1} cm^{-1}$)	A ($cm^3 g^{-1}$ molec)	C_P (cal K^{-1} $mole^{-1}$)
NO_2	4.68[b]	146.3[b]	4.24×10^{-10}	3.890×10^{-5}[a]	6.28[a]	8.79[a]
He	2.551[a]	10.22[a]		3.512×10^{-4}[d]	0.517[e]	2.5 R[c]
Ne	2.82[a]	32.8[a]		1.153×10^{-4}[d]	0.997[e]	2.5 R[c]
Ar	3.542[a]	93.3[a]	3.19×10^{-10}	4.165×10^{-5}[d]	4.143[e]	2.5 R[c]
Kr	3.655[a]	178.9[a]	3.03×10^{-10}	2.250×10^{-5}[c]	6.256[e]	2.5 R[c]
Xe	4.047[a]	231.0[a]	3.21×10^{-10}	1.300×10^{-5}[c]	10.155[e]	2.5 R[c]

[a] Ref. 24.
[b] Ref. 25.
[c] Ref. 21.
[d] Ref. 26.
[e] Ref. 27.

energy deposition occurs in a time scale that is shorter than the acoustic transit time; if the acoustic time were shorter, no spike would be seen.[13]

The small perturbations in Fig. 2 at 273 μs for Ar and at 396 μs for Kr are due to returning acoustic waves, which were reflected from the cell walls; a reflected acoustic wave for Xe in our cell occurs at 495 μs. Even if the reflected acoustic waves have no particular significance in our experiments, it is interesting to note that if the laser beams are located slightly off the cell axis, the observed acoustic wave perturbations for the first reflection (and all subsequent odd numbered reflections) tends to a focus away from the optical axis, while the second reflection (and all subsequent even numbered reflections) focuses at the original optical axis. In most experiments, only the even numbered acoustic reflections produced significant TDTL signals, due to this effect.

V. BEAM SIZE DETERMINATION

The characterization of the laser beam is important because the initial spatial distribution of the excited molecules is determined by the spatial distribution of the laser beam, as well as the time constants for acoustic waves, thermal conductivity and diffusion, as discussed earlier. In all the simulations reported here, the spatial profile of the laser was assumed to be Gaussian and the beam size parameter r_b was determined on that basis from the experimental data. For a Gaussian beam, r_b is the radius at which the intensity drops to $1/e$ of the intensity at beam center. For highest accuracy thermal lensing measurements, very high quality Gaussian laser beams are desirable, but for most pulsed tunable dye lasers, the beams are clearly not Gaussian. Even if the laser beam is Gaussian, beam size measurements require data of high precision. Given these difficulties, it is often more practicable to determine r_b by using a standard gas of known thermal conductivity coefficient, and calculating r_b from the observed time for thermal conductivity. If the laser beam is non-Gaussian, r_b loses its physical significance and merely becomes a fitting parameter.

In our experiments for each inert gas, we measured the TDTL signal at high pressures and for very long times where the decay of the lens is controlled by thermal conductivity. For these conditions, Bailey *et al.*[21] have shown that a plot of Eq. (19) allows determination of τ_c for a Gaussian laser beam:

$$[(1-S)^{-1/2}-1]^{-1/2} = (t+\tau_c)C, \tag{19}$$

where C is a constant.

Using Eq. (5), r_b can be determined from τ_c, provided that the thermal conductivity coefficient for the gas mixture is known. In Fig. 3 we show a plot of the left side of Eq. (19) vs time for 498 Torr of Xe and 0.098 Torr of NO_2, and the data are well represented by Eq. (19) [from the observed decay, $r_b = 0.072$ cm]. If Fig. 3 had shown some curvature at the earliest times, that may have been an indication that energy transfer is still playing a role at the long times and high pressure of the experiment. The procedure just outlined was carried out each day for pressures at which thermal conductivity was the controlling factor. Typically, beam radius for the experiments averaged 0.072 ± 0.005 cm.

Some simulations were carried out for assumed non-Gaussian profiles. The simulated TDTL signals that resulted were plotted according to Eq. (19) and it was found that the plots were linear, despite the non-Gaussian profile. Thus, curvature in the plot is not a diagnostic for beam profile. Moreover, the assumed non-Gaussian profiles did not lead to significant differences in derived energy transfer param-

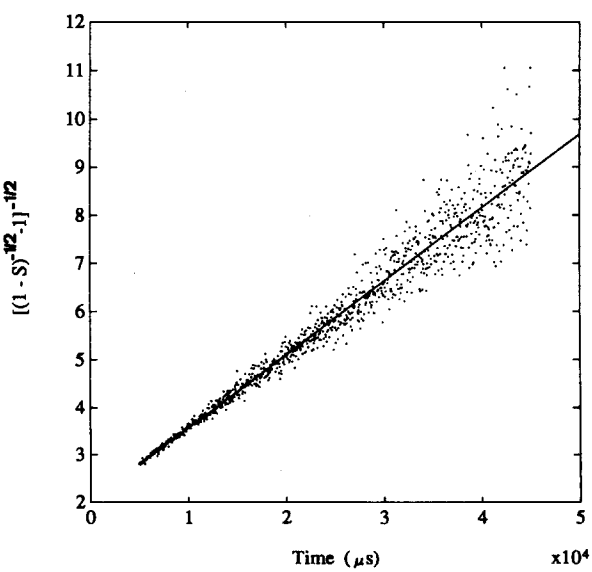

FIG. 3. Plot of $[(1-S)^{-1/2}-1]^{-1/2}$ vs time for an experiment with 498 Torr of Xe and 0.098 Torr of NO_2.

eters, and thus Gaussian profiles were assumed in all subsequent analysis.

VI. ENERGY TRANSFER RESULTS

Figure 4 shows typical TDTL signals for several gas pressures, holding the NO_2/Kr mixing ratio constant at $\sim 1/5000$ to minimize the effects of NO_2–NO_2 collisions. Also shown in Fig. 4 are theoretical simulations using the same time-dependent bimolecular rate constants at all the pressures, demonstrating the consistency of the results. The general shapes of the TDTL signals are very well reproduced for this particular set of energy transfer parameters, although for some of the pressures it is possible to find a better fit. Similar experiments and simulations have been carried out for Ar and Xe, using the same range of pressures and the same dilution ratio. For each of the inert collider gases it is possible to simulate all the signals with a set of energy transfer parameters characteristic of the particular collider. Also needed in the simulations are estimates of the fraction of excited molecules, which depends on the pump laser energy and the absorption cross section, which was taken to be 5×10^{-19} cm^2.[28] Experiments were also carried out for larger NO_2 mixing ratios in order to determine the rate constant for NO_2^*–NO_2 collisions. The simulation rate constants, experimental laser energy measurements, and beam size parameters r_b that produce the best fits for Ar, Kr, and Xe runs are presented in Table II.

The sensitivity of the simulation parameters was determined by varying assumed values for 1) the beam size, 2) the values of the rate constant, and 3) the functional form of k_e. The effect of the beam size is particularly important in simulating the decay of the signal at low and moderate pressures,

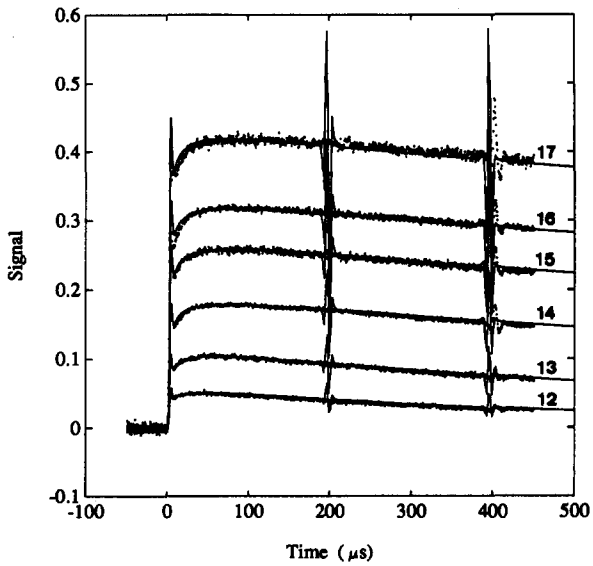

FIG. 4. Experimental and calculated TDTL signals for excited NO_2 in Kr. The simulations have been done using the energy transfer rate constant corresponding to run 12 in Table II. See Table II for the curve labels and for the physical conditions of these calculations.

TABLE II. Energy transfer parameters[a]

#	Gas	P(Torr)	NO_2(Torr)	k_o	A	k_1	B	k_{lim}	E_{laser} (mJ)	r_b (cm)
1	Ar	47.68	0.0093	5.82E − 13	0.004	1.07E − 14	0.00004	1.78E − 15	2.74	0.0788
2	Ar	99.12	0.019	5.60E − 13	0.004	1.03E − 14	0.00004	1.71E − 15	2.80	0.0788
3	Ar	199.96	0.039	5.55E − 13	0.004	9.26E − 15	0.00005	1.39E − 15	2.96	0.0788
4	Ar	299.94	0.059	5.55E − 13	0.004	9.26E − 15	0.00004	1.54E − 15	3.12	0.0850
5	Ar	399.92	0.078	5.55E − 13	0.004	9.18E − 15	0.00004	1.54E − 15	3.08	0.0788
6	Ar	500	0.098	5.55E − 13	0.004	1.02E − 14	0.00004	1.70E − 15	3.08	0.0788
7	Ar	38.17	0.079	6.10E − 13	0.004	2.02E − 14	0.00004	4.36E − 15	3.64	0.0788
8	Ar	14.68	0.079	6.09E − 13	0.004	4.41E − 14	0.00004	1.05E − 14	3.68	0.0788
9	Ar	61.72	0.079	6.00E − 13	0.004	1.57E − 14	0.00004	3.60E − 15	3.68	0.0767
10	Kr	92.62	0.072	5.99E − 13	0.004	1.73E − 14	0.00004	2.86E − 15	4.48	0.0767
11	Kr	25.25	0.005	9.16E − 13	0.004	1.22E − 14	0.00004	2.44E − 15	0.53	0.0670
12	Kr	50.48	0.0099	9.17E − 13	0.004	1.22E − 14	0.00004	2.44E − 15	4.20	0.0670
13	Kr	102.46	0.0202	9.03E − 13	0.004	1.20E − 14	0.00004	2.41E − 15	4.56	0.0640
14	Kr	198.46	0.0391	9.33E − 13	0.004	1.24E − 14	0.00004	2.49E − 15	3.56	0.0670
15	Kr	302.94	0.0597	9.16E − 13	0.004	1.22E − 14	0.00004	2.44E − 15	1.40	0.0670
16	Kr	385.92	0.076	9.23E − 13	0.004	1.23E − 14	0.00004	2.46E − 15	1.52	0.0670
17	Kr	497	0.098	7.76E − 13	0.005	1.24E − 14	0.00004	2.48E − 15	0.53	0.0670
18	Xe	25.13	0.0049	9.21E − 13	0.004	1.23E − 14	0.00004	2.45E − 15	1.92	0.0729
19	Xe	50.23	0.0099	9.21E − 13	0.004	1.23E − 14	0.00004	2.46E − 15	4.72	0.0680
20	Xe	100.17	0.0197	9.24E − 13	0.004	1.23E − 14	0.00004	2.46E − 15	1.46	0.0680
21	Xe	200.91	0.0395	9.21E − 13	0.004	1.23E − 14	0.00004	2.46E − 15	0.70	0.0729
22	Xe	299.89	0.059	9.26E − 13	0.004	1.23E − 14	0.00004	2.47E − 15	0.72	0.0729
23	Xe	402.87	0.0792	9.19E − 13	0.004	1.23E − 14	0.00004	2.45E − 15	0.75	0.0729
24	Xe	487.85	0.098	7.90E − 13	0.005	1.26E − 14	0.00004	2.53E − 15	0.78	0.0729
25	Xe	30.16	0.16	8.18E − 13	0.004	4.24E − 14	0.00004	1.02E − 14	0.84	0.0650
26	Xe	50.23	0.16	9.21E − 13	0.004	2.95E − 14	0.00004	7.25E − 15	0.51	0.0650
27	Xe	11.1	0.16	7.78E − 13	0.004	1.17E − 13	0.00004	2.75E − 14	1.18	0.0700
28	Xe	99.4	0.16	8.67E − 13	0.0045	2.11E − 14	0.00004	4.65E − 15	0.40	0.0729
29	Xe	50.57	0.0814	9.13E − 13	0.004	2.07E − 14	0.00004	4.81E − 15	0.36	0.0729

[a] k_e in units of cm^3 s^{-1}. Excitation energy: 21 631 cm^{-1}, T = 298 K; cell length: 89 cm, cell radius: 2.19 cm.

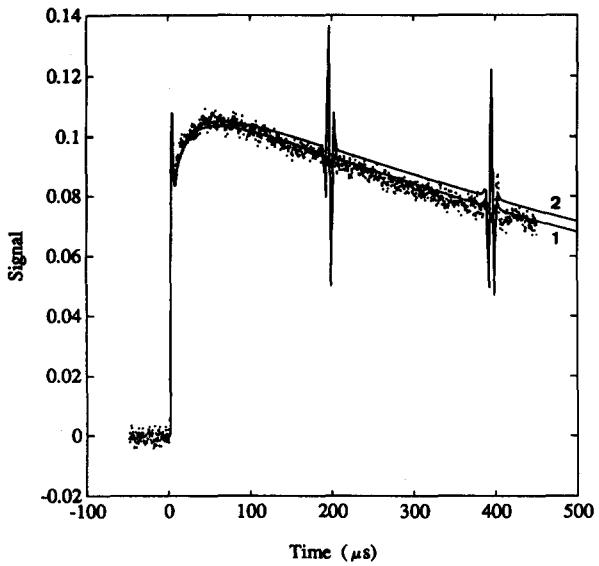

FIG. 5. Effect of a variation in the size of the laser beam on the calculated TDTL signal. 1) $r_b = 0.067$ cm, 2) $r_b = 0.064$ cm. See Table II, run 13 for pressure conditions and energy transfer parameters.

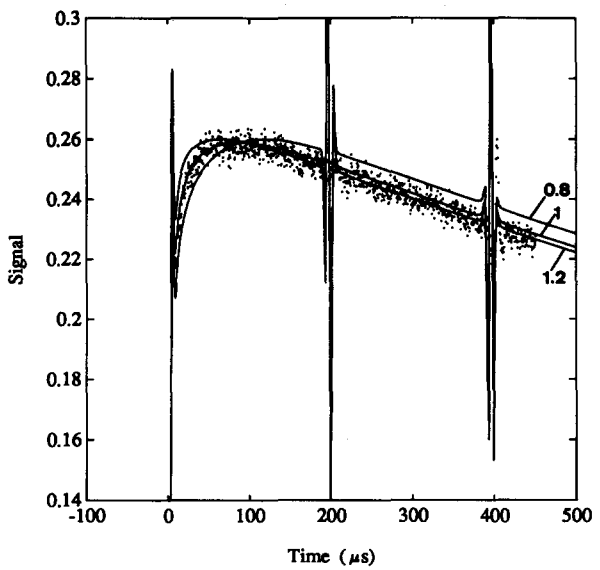

FIG. 7. The same as Fig. 6, but for 0.0597 Torr of NO_2 and 302.94 Torr of Kr. Run 15 in Table II.

as illustrated in Fig. 5 for Experiment 13 (see Table II for conditions). The 5% change in r_b clearly degrades the simulation. The maximum change in r_b necesary to produce a good fit to any of the experimental signals was only 5%. At higher pressure and for time scales in which energy transfer is playing a more important role, the sensitivity to r_b is less important.

Figures 6–8 illustrate the effects of changing the bimolecular rate constant in simulations of experiments at three different pressures. In each case, the best fit k_e was multiplied by factors of 1.2 and 0.8, in order to determine sensitivity to variations in the fitted rate constant. Inspection of the figures shows that the fit is very sensitive to variations in k_e. For each of the three pressures, the 20% variation is the maximum change that will still produce an acceptable fit.

It is interesting to analyze in some detail how the signals are affected by the different terms in Eq. (18). The rising part of the signal and the position of the spike are controlled mostly by the first term. In particular the ratio k_o/A controls the amount of energy that has been deposited in the time period in which the acoustic effects are competing with energy transfer. For a good fit, the ratio was found to be highly constrained.

Note that in our simulations the position of the spike has been reproduced correctly, but the magnitude of the spike in the calculated signal is in general overestimated to a small

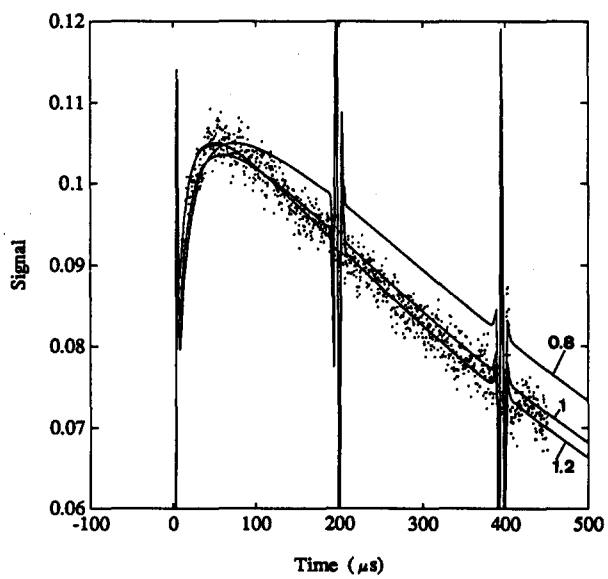

FIG. 6. Effect of a 20% change in the rate constant for energy transfer on the calculated TDTL signal for NO_2 (0.0202 Torr) in Kr (102.46 Torr). The curve labels indicate the factor for which k_e has been multiplied with respect to k_e in Table II (run 13).

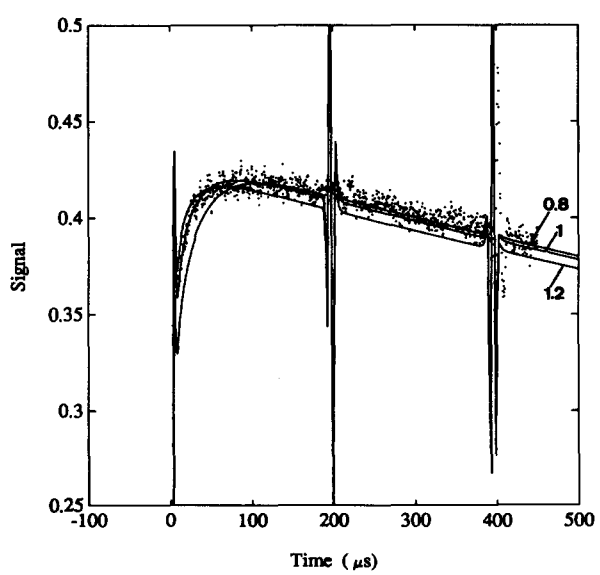

FIG. 8. The same as Fig. 6, but for 0.098 Torr of NO_2 and 497 Torr of Kr. Run 17 in Table II.

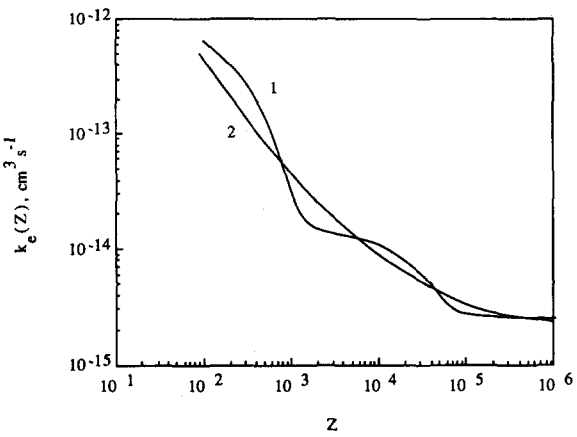

FIG. 9. Example of the functional form for the energy transfer rate constant $k_e(Z)$ for the deactivation of NO_2 by Ar, Kr or Xe, in units of $cm^3 s^{-1}$. (corresponding to run 14 in Table II.) 1) Eq. (18). 2) Smoothed $k_e(Z)$; see text for details.

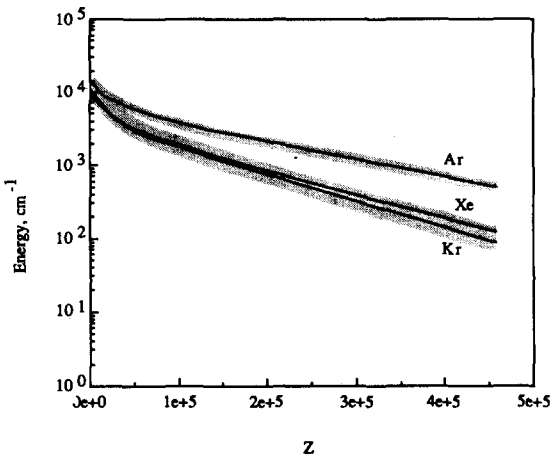

FIG. 10. Dependence of the energy content of excited NO_2 with the number of collisions (Z) for Kr, Xe, and Ar.

extent. This problem is likely due to imperfections in the shape of the laser beam, as discussed above. Following the spike, the slowly rising signal and the position of the broad maximum are controlled by the second and third terms in Eq. (18): a fast rate constant shifts the maximum to shorter times and increases the slope of the rising signal. The term that dominates will, in general, depend on the total pressure. The effects of the third term in Eq. (18) are also seen at low pressures, where the decay of the signal is controlled by this term and by the size of the laser beam.

The sensitivity of the simulations to the assumed functional form of the rate constant was also investigated. The sum of exponential factors [Eq. (18)] reproduces all the characteristics of the TDTL signal, but the rate constant exhibits a series of "steps", which may, or may not be physically significant. To determine whether the "steps" are significant, a smoother function was substituted and simulations were carried out. The smoother function was obtained by a second order polynomial least squares fit of $\ln(k_e)$ vs $\ln(Z)$, where $Z = \omega t$, the number of collisions, as shown in Fig. 9. Simulations carried out using the smoother version of k_e also reproduced the major features of the TDTL signals, and thus the "steps" are an artifact due to the assumed form for k_e and have no real significance.

TABLE III. Recommended energy transfer rate constants[a] and $\langle\langle \Delta E \rangle\rangle$ parameters[b]

Collider	k_o	A	k_1	B	k_{lim}
Ar	$5.82E-13$	0.004	$1.07E-14$	0.00004	$1.78E-15$
Kr	$9.33E-13$	0.004	$1.24E-14$	0.00004	$2.49E-15$
Xe	$9.21E-13$	0.004	$1.23E-14$	0.00004	$2.46E-15$

[a] k_e (in $cm^3 s^{-1}$) $= k_o \exp(-A\omega t) + k_1 \exp(-B\omega t) + k_{\text{lim}}$.
[b] $\langle\langle \Delta E(t) \rangle\rangle = k_e(t)E(t)/\omega$ and $E(t) = H_1 \exp\{[(k_o/A\omega)(\exp(-A\omega t) - 1)] + [(k_1/B\omega)(\exp(-B\omega t) - 1)] - k_{\text{lim}} t\}$, where $H_1 = 21\,631$ cm^{-1}. For the uncertainties in the $\langle\langle \Delta E \rangle\rangle$ values derived from these parameters, see the discussion in the text.

VII. DISCUSSION

Deactivation by Inert Gases

From simulations of each experimental run in Table II, values for $k_e(t)$ were obtained, each with an uncertainty of $\sim 20\%$. A careful examination of the data showed that a single "global" expression for $k_e(t)$ simulates the complete set of measurements for a single collider gas, if small discrepancies are accepted for the first few microseconds of the signals. This is acceptable, because the laser beams are non-Gaussian and the initial gas-dynamic relaxation is not accurately described by the theory described above. The initial gas-dynamic relaxation tends to produce an axially symmetric Gaussian profile, and the simulations should become more accurate at later times. The global expressions for $k_e(t)$ are presented in Table III.

From Eq. (14) and the global expressions for $k_e(t)$, the bulk average vibrational energy $\langle\langle E(t) \rangle\rangle$ in the excited NO_2 can be calculated, as shown in Fig. 10, as a function of the number of collisions Z for each collider gas. The shaded area in the figure represents the estimated uncertainties in $\langle\langle E(Z) \rangle\rangle$. From Eq. (17), the time-dependent bulk average amount of energy transferred per collision $\langle\langle \Delta E(t) \rangle\rangle$ can be calculated and represented as a function of $\langle\langle E(t) \rangle\rangle$, as shown in Fig. 11, where the shaded area represents the estimated uncertainties.

In Fig. 11, the shapes of the curves and the magnitudes of $\langle\langle \Delta E \rangle\rangle$ are quite similar for the three inert gases, in general agreement with studies of other excited species where no significant differences were observed among the inert gases.[8,9] Note that the "kinks" in the curves are a consequence of the function used for $k_e(t)$ and have no physical significance; when the smoother function for k_e was used, the general shape of $\langle\langle \Delta E(Z) \rangle\rangle$ is the same, but the kinks are smoothed out.

The collisional deactivation of NO_2 in Fig. 11 shows a very strong dependence on vibrational energy. For energies up to ~ 4000 cm^{-1}, the energy-dependence is near linear, but it increases to an approximate quadratic dependence from ~ 4000 cm^{-1} to $\sim 10\,000$ cm^{-1}. In fact the whole re-

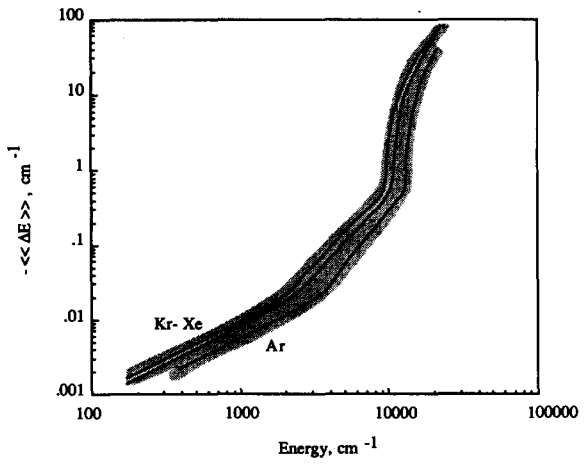

FIG. 11. Average energies $\langle\langle \Delta E \rangle\rangle$ transferred per collision of excited NO_2 with Kr, Xe, and Ar. Shading shows estimated uncertainties.

gion below 10 000 cm^{-1} could be moderately well represented by a quadratic function. At still higher energies, the results are uncertain, but it appears that the dependence is at least 5th order, and possibly larger.

The exact position of the sharp bend is difficult to assess and this fact affects the precision of the derived $\langle\langle \Delta E \rangle\rangle$ values. For example if we take the k_e values that produce the best fits for 200 and 500 Torr of Kr (see Table II) and calculate $\langle\langle \Delta E \rangle\rangle$ using Eq. (17) we find that the bend occurs at E ~ 9500 cm^{-1} for 200 Torr and at E ~ 12 000 cm^{-1} for 500 Torr. Is clear that in this particular region the derived $\langle\langle \Delta E \rangle\rangle$ are quite different leading to a large uncertainty. A comparison of the results derived from the two fits indicate an uncertainty of 20% in the $\langle\langle \Delta E \rangle\rangle$ at energies close to 21 600 cm^{-1}, a factor ~9 in the region of the sharp bend, 35% at 9000 cm^{-1}, 30% at 7000 cm^{-1}, 40% at 3000 cm^{-1}, and less than 10% at lower energies. Similar analysis for Xe leads to almost the same relative uncertainty in the $\langle\langle \Delta E \rangle\rangle$ values. The sharp bend for Ar occurs at ~12 000 cm^{-1} for all the fits and therefore the estimated uncertainty from this analysis is smaller than for Kr and Xe. It is important to remember that if the small differences between experimental and calculated signals during the first 5–10 μs are accepted, all the pressures can be fitted with the same k_e. As discussed above, these discrepancies are due in part to the non-Gaussian laser beam and therefore is probable that the errors in the region of 10 000–12 000 cm^{-1} are overestimated.

Extrapolations of the $-\langle\langle \Delta E \rangle\rangle$ curves to the dissociation energy, 25 132 cm^{-1} are quite uncertain, but nonetheless the values of ~60, 83, and 90 cm^{-1} for the colliders Ar, Xe, and Kr, respectively, were estimated. These values for $\langle\langle \Delta E \rangle\rangle$ can be compared with those obtained from low pressure thermal recombination rate constant, k_o, measurements. Unfortunately, such $\langle \Delta E \rangle$ values are determined from collision efficiencies, β_c, which are, in turn, based in theoretical calculations[29–31] of the strong collider rate constant. For example, Troe and coworkers[9] reported $\beta_c = 0.46$ for Ar (relative to C_3F_8 collider) when an extra factor of 1.7[32] is included to correct for the effects of the electronic excited states. This β_c value corresponds to $-\langle \Delta E \rangle = 300$ cm^{-1}; other evaluations produce even larger magnitudes for $\langle \Delta E \rangle$.[33] The present experimental measurements indicate that $\langle \Delta E \rangle$ magnitudes derived from the unimolecular reaction studies are significantly overestimated, probably reflecting errors in the theoretical models. One point of particular concern is the contribution of electronic excited states.[31,32]

A more detailed comparison can be made with nonreactive systems that have been investigated recently by physical methods. In large polyatomic systems, the energy-dependence of $\langle\langle \Delta E \rangle\rangle$ is much weaker, tending to be approximately first order in energy.[30] In the triatomic systems SO_2[8] and CS_2,[9] an approximate quadratic dependence was observed for deactivation by the rare gases. It is also noteworthy that the magnitudes of $\langle\langle \Delta E \rangle\rangle$ are unusually large for NO_2 deactivation, especially at low energies. Thus, both the energy dependence and the magnitudes of $\langle\langle \Delta E \rangle\rangle$ for NO_2 are distinctive, just as the NO_2 molecular properties are distinctive.

As has been mentioned earlier, several NO_2 electronic excited states are strongly coupled with the ground state. This coupling has been invoked to explain the complexity in the spectrum of NO_2 and the long lifetime for the visible fluorescence. Following light absorption, NO_2 is initially prepared in the $^2B_2$ electronic excited state, but after a short time, or a few collisions, the system undergoes internal conversion to the electronic ground state; the subsequent collisional deactivation is dominated by the ground state. The triatomics CS_2 and SO_2 also have strongly coupled electronic states and they have been found to have similar behavior.

The electronic structure of NO_2 has been investigated in several theoretical studies. According to Gillespie *et al.*,[34] there are three electronic excited states at energies below the dissociation energy for NO_2: the $^2B_2$ state origin is near 9520 cm^{-1}, the $^2B_1$ near 13 390 cm^{-1}, and the $^2A_2$ state near 14 841 cm^{-1}. Experimentally the origin of the first electronic excited state has been located at 11 963 cm^{-1},[35] more than 2400 cm^{-1} higher than the calculated origin, but there is no question that around 10 000–12 000 cm^{-1} the system changes dramatically. Gillespie's calculations show that NO_2 is strongly coupled vibronically due to the fact that the ground and excited states have different bond angles, resulting in a large vibrational-overlap Franck–Condon factor. In this case, and even if the density of states is rather low (sparse case, according to Bixon and Jortner[36]), extensive mixing can still take place. It is likely that the TDTL energy transfer results are closely related with this fact.

To understand qualitatively the sharp bend in ΔE around 10 000–12 000 cm^{-1}, it is useful to consider the electronic energy as a function of bond angle for the low-lying electronic states of NO_2 (Fig. 12).[34] At the initial energy of our experiment (21 631 cm^{-1}), the amplitude of the motion can be very large (broken line in Fig. 12). Due to the strong coupling, it is likely that the system can cross freely from one potential energy surface to another, without significant trapping on any one surface. The large amplitude of vibration probably produces a very low frequency of the motion, which will favor V–T energy transfer. Predictions of SSH theory indicate that the lower the frequency, the higher the

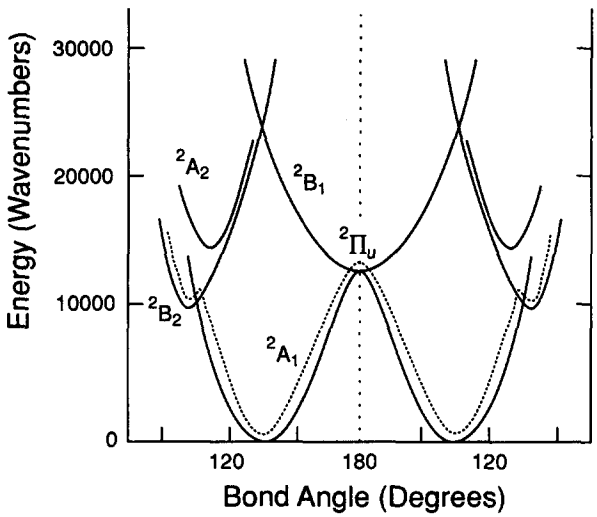

FIG. 12. Schematic of the electronic energy as a function of bond angle for the low-lying electronic states of NO_2 (adapted from Ref. 34).

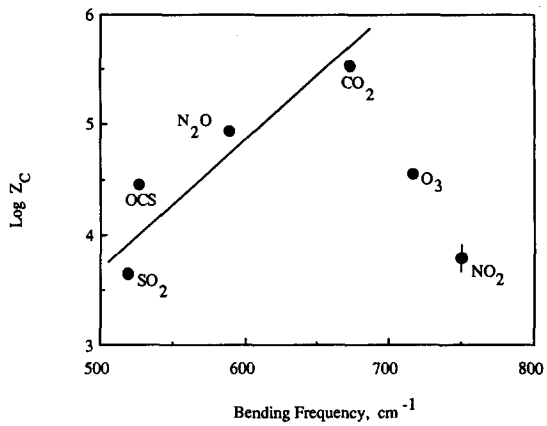

FIG. 13. Lambert-Salter plot for Ar-triatomic molecules: NO_2 (this work), O_3 (Ref. 44), CO_2 (Ref. 45), N_2O (Ref. 45), OCS (Ref. 46), and SO_2 (Ref. 47).

probability for deactivation, because the collision will provide more Fourier components at low vibrational frequencies.[37] As the system energy is reduced, the NO_2 bending motion becomes more and more restricted, until below the energy of the first electronic excited state the motion is confined to the lowest potential energy surface. The other internal degrees of freedom are also likely to exhibit larger amplitude motions at high energy than at low energy, due to the same effects. Thus, the probability of V–T transfer will decrease markedly at lower energies. Quantitative estimates of this effect will require accurate potential surfaces and good methods for treating the couplings among the excited states.

Near the end of the energy cascade, the remaining excited NO_2 is expected to reside mostly in the (010) state, and the corresponding energy transfer can be compared with V–T energy transfer measured, for example, in ultrasonic attenuation experiments. At low energy, the observed $k_e(t)$ becomes a constant ($k_{\rm lim}$) and $\langle\langle \Delta E \rangle\rangle$ becomes a linear function of ensemble average energy, consistent with this view. If we equate the rate of energy deposition from our experiments to that expected from V–T transfer involving the (010) state, we can write

$$\frac{dq}{dt} = -\frac{d}{dt}\langle\langle E \rangle\rangle = k_{VT} N^* E_{010}, \tag{20}$$

where k_{VT} is the V–T rate constant from the (010) state, E_{010} is the energy of the state, and N^* is the population in the state. The ensemble average energy in the (010) state is just

$$\langle\langle E \rangle\rangle_{010} = N^* E_{010}. \tag{21}$$

If we assume that all of the excited molecules near the end of the energy cascade are in the (010) state, then $N^* = N_1$. Using Eq. (14), we obtain

$$k_{VT} = \frac{H_1}{E_{010}} k_{\rm lim}. \tag{22}$$

The energy ratio in Eq. (22) is 21 631/750 = 28.8. Thus the V–T rate constant for deactivation of the (010) state is estimated to be $\sim (5.1 \pm 1.0) \times 10^{-14}$ cm^3 s^{-1} for argon. This rate constant corresponds to a total number of collisions needed for deactivation:

$$Z_C = k_{\rm LJ}/k_{VT} = 6200. \tag{23}$$

In Fig. 13, Z_C is compared with corresponding values for deactivation by argon of several other triatomics, and it is clear that the NO_2 rate constant is unusually large in magnitude. A possible explanation for this anomalous behavior is related to the fact that NO_2 is a free radical and each energy level is split into two spin components. As discussed by Nikitin,[38] a possible cause for the high efficiency of the vibrational relaxation of NO and some other molecules with incompletely filled electron shells is the nonadiabaticity of vibrational excitation during collisions. He pointed out that when one or both colliding partners are in a degenerate electronic state, intermolecular interactions lift the electronic degeneracy, so that when molecules approach, there arise a whole set of adiabatic potential energy surfaces which are strongly coupled. Two such states are shown schematically in Fig. 14 (adapted from Nikitin's work). Nonadiabatic transitions provide additional paths of energy transfer that can greatly enhance the V–T energy transfer cross section. Molecules approaching on the solid curve corresponding to $v = 1$ can reach an inner turning point and be reflected, only

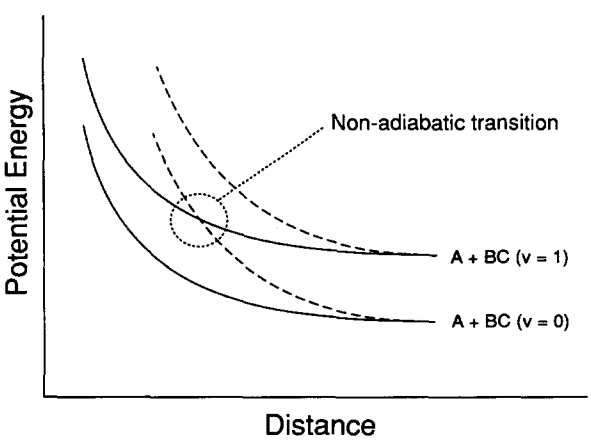

FIG. 14. Schematic of potential energy vs distance for an open shell molecule (adapted from Ref. 38).

to encounter the nonadiabatic transition indicated in the figure, and switch to the $v = 0$ potential curve. This mechanism is present at all energies for NO_2, and at higher energies its effect is combined with that due to the large amplitude vibrational motion to produce the very large magnitudes of $\langle\langle \Delta E \rangle\rangle$ observed.

Deactivation by unexcited NO_2

By varying the mixing ratio in the NO_2–Ar and NO_2–Xe systems, $\langle\langle \Delta E \rangle\rangle$ can be estimated for V–T energy transfer from excited NO_2 to unexcited NO_2, and the results are shown in Fig. 15. These results may be uncertain by as much as a factor 2, nonetheless is possible to make some interesting comparisons with other studies involving NO_2^*–NO_2 energy transfer. Kaufman[20] and coworkers, in their low pressure fluorescence studies at excitation energies ranging from 18 800 to 24 700 cm^{-1}, estimated the step size for the average energy transferred per collision from a model calculation: $\langle\langle \Delta E \rangle\rangle = -1000 \pm 500$ cm^{-1} for NO_2^*–NO_2 collisions at $E = 18\,365$ cm^{-1}. Even larger values were reported by Schwartz and Johnston[39] in similar experiments. From our measurements we calculate $\langle\langle \Delta E \rangle\rangle = -1040$ cm^{-1} at $E = 18\,365$ cm^{-1}, in good agreement with the fluorescence studies, especially considering the uncertainties in the respective measurements. Since the TDTL technique is only sensitive to V–T energy transfer and the fluorescence experiments measure total energy transfer, the good agreement between the two techniques may be an indication that V–T transfer is one of the most important paths for highly excited NO_2. This conclusion is consistent with the recent finding of inefficient V–V energy transfer from excited NO_2 to ν_3 of CO_2.[40]

The conclusion that V–T transfer is a major pathway for deactivation in NO_2^*–NO_2 collisions is somewhat surprising at first glance, because NO_2 can react to produce N_2O_4, which is weakly bound chemically. One might expect the chemically bound $N_2O_4^*$ to have a lifetime long enough before redissociation for vibrational energy to completely randomize and be shared equally between the two NO_2 molecules after they have separated. If this model is correct, the probability of forming a "strong complex" is given by the ratio of k_{rec}/k_{LJ}, where the recombination rate constant is at the high pressure limit. If each "strong complex" results in half the excitation energy being lost during each collision (complete energy randomization) then the bulk average energy transferred per collision is given by

$$-\langle\langle \Delta E \rangle\rangle_{model} = \frac{1}{2}\frac{k_{rec}}{k_{LJ}}\langle\langle E \rangle\rangle. \tag{24}$$

Taking k_{rec} from the work of Cobos and Troe,[41] $\langle\langle \Delta E \rangle\rangle_{model} \approx -18$ cm^{-1}, when $\langle\langle E \rangle\rangle = 18\,365$ cm^{-1}. This energy transfer would be mostly V–V transfer, which does not produce TDTL signals. This quantity is small, compared with the total $\langle\langle \Delta E \rangle\rangle$ observed in both the fluorescence quenching experiments and the TDTL measurements, and therefore is consistent with the majority of deactivation occurring through V–T energy transfer.

It is also possible to compare our results for the NO_2^*–NO_2 deactivation with a model calculation presented by Adler-Golden[42] to interpret the NO_2 chemiluminescence. He assumed a coarse-grained stepladder model with energy levels separated by 1000 cm^{-1}. By solving a system of linear equations he evaluated the rate constant $k_M(i,j)$ for collisional energy transfer from the grain i to j, this rate constant can be related to $\langle\langle \Delta E \rangle\rangle$ using the relation

$$\langle\langle \Delta E \rangle\rangle = \frac{k_M(i,j)}{k_{LJ}} \times 1000\ cm^{-1}. \tag{25}$$

The derived $\langle\langle \Delta E \rangle\rangle$ values are about a factor of three smaller than our experimental values for energies in the range from 5000 to 21 000 cm^{-1}, but at 1000 cm^{-1}, the difference is only ~20%.

In recent infrared fluorescence experiments, McAndrew *et al.*[10] measured collisional energy transfer involving the asymmetric stretching mode of NO_2 subsequent to excitation with a tunable dye laser. Unfortunately, the infrared intensities depend on unknown populations in the specific NO_2 excited states, and so it was impossible to make a detailed quantitative analysis of the results. Despite the difficulties, McAndrew *et al.* reached the conclusion that the energy-transfer rate probably exhibits an energy-dependence. Their conclusion is consistent with the results obtained in the present work, although a detailed comparison is not possible.

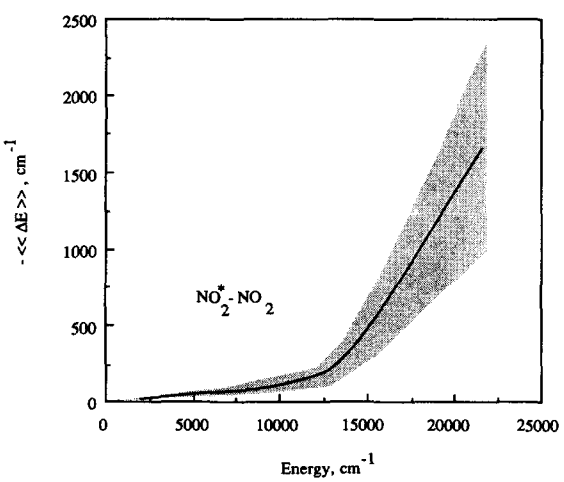

FIG. 15. The same as Fig. 11, but for NO_2 collider gas.

VIII. CONCLUSIONS

In this work we have presented a detailed study of V–T energy transfer in excited NO_2. The results show that $\langle\langle \Delta E \rangle\rangle$ for this system exhibits a very strong energy dependence of the average energy transferred per collision, even stronger than the quadratic dependence observed for CS_2 and SO_2. Moreover, $\langle\langle \Delta E \rangle\rangle$ changes dramatically at energies near the origins of the excited electronic states. This behavior can be explained as due to enhancement of V–T transfer by the large amplitude vibrational motions associated with the coupled electronic states. The $\langle\langle \Delta E \rangle\rangle$ values at low energy were related to the V–T energy transfer rate constant for deactivation of the (010) state, and the large magnitude of this rate constant can be explained by Nikitin's

model for nonadiabatic couplings in systems with degenerate electronic states.

An important strength of the TDTL technique is that the complex spectroscopy associated with NO_2 can be avoided. It would be of value to compare the results obtained here with those obtained using other techniques, however, in order to identify possible systematic errors.

A very useful adjunct to the present work would be trajectory calculations, perhaps similar to those for CS_2.[43] This will require developing methods for dealing with multiple coupled electronic states and nonadiabatic transitions, in order to describe NO_2 realistically.

ACKNOWLEDGMENTS

This work was funded by the U.S. Department of Energy, Office of Basic Energy Sciences. B.M.T. thanks CONICET of Argentina for a postdoctoral fellowship, and T. L. W thanks NSF for an undergraduate fellowship as part of the Research Experiences for Undergraduates program in the Department of Atmospheric, Oceanic, and Space Sciences (Grant ATM-8712631). Thanks also go to S. J. Jacobs for providing a copy of the program DIFCOLL and for discussions and assistance with the solution of the hydrodynamic equations.

[1]J. Shi and J. R. Barker, J. Chem. Phys. **88**, 6219 (1988).
[2]J. Shi, D. Bernfeld, and J. R. Barker, J. Chem. Phys. **88**, 6211 (1988).
[3]J. M. Zellweger, T. C. Brown, and J. R. Barker, J. Chem. Phys. **83**, 6261 (1985).
[4]M. L. Yerram, J. D. Brenner, K. D. King, and J. R. Barker, J. Phys. Chem. (to be published).
[5]H. Hippler, J. Troe, and J. Wendelken, J. Chem. Phys. **78**, 6709, 6718 (1983).
[6]H. Hippler, L. Lindemann, and J. Troe, J. Chem. Phys. **83**, 3906 (1985).
[7]B. Abel, B. Herzog, H. Hippler, and J. Troe, J. Chem. Phys. **91**, 900 (1989).
[8]M. Heymann, H. Hippler, D. Nahr, H. J. Plach, and J. Troe, J. Phys. Chem. **92**, 5507 (1988).
[9]J. E. Dove, H. Hippler, and J. Troe, J. Chem. Phys. **82**, 1907 (1985); M. Heymann, H. Hippler, H. J. Plach, and J. Troe, J. Chem. Phys. **87**, 3867 (1987).
[10]J. J. F. McAndrew, J. M. Preses, R. E. Weston, and G. W. Flynn, J. Chem. Phys. **90**, 4772 (1989).
[11]F. R. Grabiner, D. R. Siebert, and G. W. Flynn, Chem. Phys. Lett. **17**, 189 (1972); D. R. Siebert, F. R. Grabiner, and G. W. Flynn, J. Chem. Phys. **60**, 1564 (1974).
[12]J. R. Barker and T. Rothem, Chem. Phys. **68**, 331 (1982); P. L. Trevor, T. Rothem, and J. R. Barker, *ibid.* **68**, 341 (1982).
[13]J. R. Barker and B. M. Toselli, *Photothermal Investigations of Solids and Fluids*, edited by Jeffrey A. Sell (Academic, New York, 1989), Chap. V.
[14]R. T. Bailey, F. R. Cruickshank, D. Pugh, and K. Middleton, J. Chem. Soc. Faraday II **81**, 255 (1985); R. T. Bailey, F. R. Cruickshank, R. Guthrie, D. Pugh, and I. J. M. Weir, Chem. Phys. **114**, 411 (1987).
[15]N. Presser, J. R. Barker, and R. J. Gordon, J. Chem. Phys. **78**, 2163 (1983); K. M. Beck, A. Ringwelski, and R. J. Gordon, Chem. Phys. Lett. **121**, 529 (1985); K. M. Beck and R. J. Gordon, J. Chem. Phys. **89**, 5560 (1988).
[16]T. J. Wallington, M. D. Scheer, and W. Braun, Chem. Phys. Lett. **138**, 538 (1987).
[17]H. Sontag, A. C. Tam, and P. Hess, J. Chem. Phys. **86**, 3950 (1987).
[18]D. K. Hsu, D. M. Monts, and R. N. Zare, in *Spectral Atlas Of Nitrogen Dioxide 5530 to 6480 Å* (Academic, New York, 1978).
[19]A. E. Douglas, J. Chem. Phys. **45**, 1007 (1966).
[20]L. F. Keyser, S. Z. Levine, and F. Kaufman, J. Chem. Phys. **54**, 355 (1971); V. M. Donnelly and F. Kaufman, J. Chem. Phys. **66**, 4100 (1977); V. M. Donnelly, D. G. Keil, and F. Kaufman, J. Chem. Phys. **71**, 659 (1979).
[21]R. T. Bailey, F. R. Cruickshank, D. Pugh, and W. Johnstone, J. C. S. Faraday II, **76**, 633 (1980); R. T. Bailey, F. R. Cruickshank, R. Guthrie, D. Pugh, and I. J. M. Weir, Mol. Phys. **48**, 81 (1983); R. T. Bailey, F. R. Cruickshank, D. Pugh, A. McLeod, and W. Johnstone, Chem. Phys. **68**, 351 (1982).
[22]S. J. Jacobs, Chem. Phys. **132**, 71 (1989).
[23]M. Born and E. Wolf, *Principles of Optics* (Pergamon, New York, 1975), p. 88.
[24]R. C. Reid and T. K. Sherwood, *The Properties of Gases and Liquids* (McGraw-Hill, New York, 1966).
[25]J. Troe, J. Chem. Phys. **66**, 4758 (1977).
[26]C. L. Yaws, *Physical Properties* (McGraw-Hill, New York, 1978).
[27]E. A. Moelwyn-Hughes, *Physical Chemistry* (Pergamon, Oxford, 1961), p. 383.
[28]A. M. Bass, A. E. Ledford, and A. H. Laufer, J. Res. Nat. Bur. Stand. **80A**, 143 (1976).
[29]J. Troe, J. Chem. Phys. **66**, 4745 (1977).
[30]I. Oref and D. C. Tardy, Chem. Rev. (to be published).
[31]B. M. Toselli and J. R. Barker, J. Chem. Phys. **91**, 2239 (1989).
[32]I. W. M. Smith, Int. J. Chem. Kinet. **16**, 423 (1984).
[33]H. Hippler, C. Schippert, and J. Troe, Int. J. Chem. Kinet. Simp. **1**, 27 (1975).
[34]G. D. Gillespie, A. U. Khan, A. C. Wahl, R. P. Hosteny, and M. Krauss, J. Chem. Phys. **63**, 3425 (1975); G. D. Gillespie and A. U. Khan, J. Chem. Phys. **65**, 1624 (1976).
[35]J. C. D. Brand, W. H. Chan, and J. L. Hardwick, J. Mol. Spectrosc. **65**, 249 (1977).
[36]M. Bixon and J. Jortner, J. Chem. Phys. **50**, 3284 (1969).
[37]J. T. Yardley, *Introduction to Molecular Energy Transfer* (Academic, New York, 1980).
[38]E. E. Nikitin, Opt. Spectrosc. **9**, 8 (1960); E. E. Nikitin and S. Y. Umanski, Faraday Discussions Chem. Soc. **53**, 7 (1972); V. N. Kondratiev and E. E. Nikitin, *Gas-Phase Reactions* (Springer, Berlin, 1981).
[39]S. E. Schwartz and H. S. Johnston, J. Chem. Phys. **51**, 1286 (1969).
[40]J. Z. Chou, S. A. Hewitt, J. F. Hershberger, B. B. Brady, G. B. Spector, L. Chia, and G. W. Flynn, J. Chem. Phys. **91**, 5392 (1989).
[41]C. J. Cobos and J. Troe, J. Chem. Phys. **83**, 1010 (1985).
[42]S. M. Adler-Golden, J. Phys. Chem. **93**, 684, 691 (1989).
[43]M. Bruehl and G. C. Schatz, J. Chem. Phys. **89**, 770 (1988); J. Phys. Chem. **92**, 7223 (1988).
[44]J. I. Steinfeld, S. M. Adler-Golden, and J. W. Gallagher, J. Phys. Chem. Ref. Data **16**, 911 (1987).
[45]R. T. Bailey and F. R. Cruickshank, Specialist Periodical Reports **3**, 109 (1978).
[46]D. R. Siebert and G. W. Flynn, J. Chem. Phys. **64**, 4973 (1976).
[47]F. Douglas Shields, J. Chem. Phys. **46**, 1063 (1967).